New insights into the collapsing of cylindrical thin-walled tubes under axial impact load

M Shakeri*, **R Mirzaeifar,** and **S Salehghaffari**
Department of Mechanical Engineering, Amirkabir University of Technology (Tehran Polytechnics), Tehran, Iran

The manuscript was received on 25 November 2006 and was accepted after revision for publication on 8 May 2007.

DOI: 10.1243/09544062JMES562

Abstract: The current paper presents further investigations into the crushing behaviour of circular aluminium tubes subjected to axial impact load. Experiments prove that in order to achieve the real collapsing shape of tubes under axial loads in numerical simulations, an initial geometric imperfection corresponding to the plastic buckling modes should be introduced on the tube geometry before the impact event. In this study, it is shown that the collapsing shape of tube is affected by this initial imperfection and consequently it is shown that by applying an initial geometric imperfection similar to the axisymmetric plastic buckling mode, the tubes tend to collapse in a concertina mode. This phenomenon is studied for circular tubes subjected to axial impact load and two design methods are suggested to activate the axisymmetric plastic buckling mode, using an initial circumferential edge groove and using one- and two-rigid rings on the tube. In each case the broadening of the concertina collapsing region is estimated using numerical simulations. Experimental tests are performed to study the influence of cutting the edge groove on the collapsing mode.

In order to optimize the crashworthiness parameters of the structure such as the absorbed energy, maximum deflection in axial direction, maximum reaction force, and mean reaction force, a system of neural networks is designed to reproduce the crushing behaviour of the structure, which is often non-smooth and highly non-linear in terms of the design variables (diameter, thickness, and length of tube). The finite-element code ABAQUS/Explicit is used to generate the training and test sets for the neural networks. The response surface of each objective function (crashworthiness parameters) against the change of design variables is calculated and both single-objective and multi-objective optimizations are carried out using the genetic algorithm.

Keywords: axial crushing, circular tubes, plastic buckling modes, neural networks, genetic algorithm

1 INTRODUCTION

Due to the day-to-day increasing of the transport vehicles speed, traffic accidents unfortunately have become a common occurrence nowadays. In order to decrease human sufferings and financial burdens, over the last decade more focus has been paid to design the transport structures with taking the crashworthiness requirements into consideration. Many experimental and theoretical studies have been carried out on designing devices to dissipate the kinetic energy during an accident by converting this energy into another form of energy. These devices are usually called mechanical energy absorbers. Energy absorbers are classified into two major categories, the reversible energy absorbers, like the hydraulic dashpots or elastic dampers, and irreversible or collapsible energy absorbers, like energy dissipation in plastic deformation of members of the structure.

There are numerous types of irreversible energy absorbers, like circular tubes, square tubes, tubular structures, octagonal cross-section tubes, spherical shells, frusta, tapered tubes, S-shaped frames, honeycomb cells, composite tubes, foam-filled, and wood-filled tubes.

**Corresponding author: Department of Mechanical Engineering, Amirkabir University of Technology, 424 Hafez Avenue, Tehran, Iran. email: shakeri@cic.aut.ac.ir*

Thin-walled tube-like structures with circular cross-section, because of their efficiency in energy absorption and ease of manufacture represent the most common shape of collapsible energy absorbers. The kinetic energy of the accident can be dissipated in plastic deformation of tube in several forms, like inversion, splitting, mushrooming, lateral indentation, and axial crushing. Among these mechanisms, the axial crushing of circular tubes provides the best device for absorbing the kinetic energy of impact loads because of the greater amount of material participating in the plastic deformation and energy absorption. Furthermore, in the axial crushing mechanism, the reaction force is reasonably constant and the stroke length is relatively high compare with the other mechanisms of collapsing of tubes.

Circular tubes under axial quasi-static or impact load may crush in different modes, including: concertina or axisymmetric, diamond, Euler, and mixed mode. Many experimental and numerical studies have been carried out on finding the parameters that control the collapsing mode of tube under axial load. Among the performed researches, a great percent investigate the influence of geometric dimensions such as diameter, thickness, and length of the tube on the collapsing mode [**1**, **2**]. The purpose of such studies is ascertaining ranges for geometrical dimensions and then studying the collapsing mode of the tube for each range. Other than the geometrical dimensions, the influence of many other parameters is studied in the literature. For instance; the effect of mass and initial velocity of impact on collapsing of tube is studied in references [**2**] to [**4**]. Some experimental test results are reported in reference [**5**] for collapsing of tubes made of three different materials and the effects of material properties such as strain hardening and sensitivity to strain rate are studied. Controlling the collapsing shape of tube by adding stiffener rings to the tube is studied in reference [**6**] by performing experimental tests. The influence of boundary conditions at the tube wall ends and the friction coefficient is studied in reference [**7**]. The influence of the inertia characteristics of the tube on the collapsing mode is studied in reference [**8**] using a finite-element (FE) analysis. The phenomena of dynamic plastic buckling and dynamic progressive buckling are studied from the viewpoint of stress wave propagation in reference [**9**], and in reference [**10**] the FE method is used to investigate the influence of cutting a controlled size chamfer at the edge of the tube on the collapsing mode.

As a general rule, when the tube length is greater than the critical length for the given diameter and thickness, it deforms in Euler or global bending mode, which is an inefficient and unreliable mode in energy absorber designing and should be avoided in crashworthiness applications. Among the other collapsing modes besides global bending, diamond and mixed modes are the most probable collapsing modes for the common dimensions of tubes, but both of these modes have the potential ability of changing to global bending by little changes in the load or boundary conditions. Another disadvantage of collapsing in diamond or mixed mode is the high probability of miscalculations in designing tubes as shock absorbers. Because the exact collapsed shape of tube in this case is almost unpredictable even when all the external conditions (like load and boundary conditions) are known exactly. Contrary to the mentioned modes, the concertina collapsing mode is the most desired design in crashworthiness applications because of its reliability and efficiency in absorbing the impact energy. The high efficiency in energy absorption for tubes that collapse in concertina mode returns to the great percent of material that contributes in energy absorption. In addition to the energy absorption performance, the reaction force for collapsing in concertina mode does not have sudden changes in contrast with diamond collapsing. A summary of empirical relations for calculating the absorbed energy and mean reaction force for different collapsing modes is presented in reference [**1**]. Experimental studies show that in the wide range of dimensions of tubes (that is shown with different L/D and D/t ratios) there is only a limited region that the crushing of tube in concertina mode is guaranteed. Unfortunately, this region is limited to the tubes with relatively small L/D and D/t ratios that have a lower ability in dissipating the impact energy compared with the larger tubes. Among the researches carried out on designing aluminium tubes as collapsible shock absorbers, almost no work is reported on designing methods to extend the region in which the axisymmetric collapsing mode is guaranteed.

In the present study, the initial geometric imperfection of plastic buckling modes in the postbuckling analysis is introduced as a new factor that can extend the concertina collapsing region. The prevailing theory on the postbuckling analysis of tubes under axial loading is applying an initial imperfection proportional to a linear combination of all the plastic buckling modes on the tube and analysing the new structure under external loads. In this work, it is shown that by applying only an initial imperfection, proportional to the axisymmetric collapsing mode instead of the traditional method, the concertina collapsing region will extend to a wider region. In order to show this effect, numerical simulations are carried out to specify the limits of concertina collapsing mode region for tubes of various diameters, lengths, and thicknesses under axial impact load and the extension of these limits by applying the initial geometric imperfection proportional to the axisymmetric plastic buckling mode on the structure is shown in the L/D–D/t diagram in the range of $20 < D/t < 100$ and $L/D < 6$.

In order to use the introduced parameter in applied design of energy absorbers, two methods are suggested to activate the axisymmetric plastic buckling mode: cutting an initial circumferential edge groove outside the tube and using one- and two-circumferential stiffeners. Performing FE simulations, the extension of the axisymmetric collapsing region after using these methods is shown in the L/D–D/t diagram.

Almost all of the reported works on designing the cylindrical tubes as impact energy absorbers are just carried out to satisfy the imposed crashworthiness requirements, whereas, nowadays, optimization becomes a necessary part of designing procedure. The optimization of the structure under crashworthiness requirements is very complex and expensive from the computational point of view because the objective function is often non-smooth and highly non-linear in terms of design variables. The optimization procedure requires repetitive and iterative validation of the selected objective function for various values of design variables. To avoid the calculation of the objective function in each iteration by computationally costly FE simulations, approximated functions may be used to simulate the crush behaviour of the structure. The response surface methodology (RMS) [**11**], and neural network systems [**12**] are the most common devices to reproduce the crush behaviour of the structure. In the present study, a system of parallel neural networks is developed to reproduce the structural behaviour during the crush phenomenon. A limited number of FE simulations are carried out to train and test the neural network systems. The remarkable preference of the presented work to most similar studies is using different neural network systems to return each crashworthiness parameter instead of using a global network to simulate all the parameters. After training the neural network systems, the response surface of selected crashworthiness parameters against the design variables are calculated and shown in graphical form. Finally, using the response surfaces developed by the neural network systems, the genetic algorithm (GA) is implemented to find the optimal configuration of tube dimensions for both single-objective (SO) and multi-objective (MO) optimizations.

2 NUMERICAL MODEL AND VERIFICATION

2.1 Description of the FE model and material properties

Numerical simulations of axial crushing of tubes under impact loading are carried out using the FE code ABAQUS/Explicit. In order to calculate the plastic buckling mode shapes, the FE code ABAQUS/Standard is used. Four-noded shell elements with reduced formulation (S4R), suitable for large strain analysis are used to model all the analysed tubes. Three integration points are used through the shell thickness to model bending. The shell thickness is set to $t = 2$ mm for all the specimens except in the cases that another thickness is mentioned. After convergence, an element size of 3 mm is found to produce suitable results. Two rigid walls are fixed to the ends of the tube. For simulating the impact load, a point mass ($m = 250$ kg) is attached to the upper rigid wall and an initial downward velocity (V_0) is defined for the wall just before the impact event. The quasi-static load is simulated by moving the upper plate with a constant velocity downward. The tube is tied to the lower rigid wall and free at the other end. The lower plate is constrained in all degrees of freedom and the upper plate is fixed in all translational and rotational degrees of freedom except the axial displacement in order to avoid the twisting of the impactor plate. The contact between the tube and rigid walls is assumed to be frictionless, but a friction coefficient equal to 0.1 is used to model the self-contact of the inner and the outer surfaces of the shell.

The material properties are defined as linear elastic followed by non-linear work hardening in the plastic region. The true static stress–strain curve of a typical aluminium alloy obtained by a standard tensile test as shown in Fig. 1 is used to introduce the approximated true stress-plastic strain data points in numerical simulations. These points are shown in Table 1. The elastic modulus of this material is 70 Gpa, the density is $\rho = 2700\,\text{kg/m}^3$ and the Poisson ratio is $\nu = 0.3$. The material is assumed to have only isotropic strain hardening and strain rate effects on the yield strength are neglected.

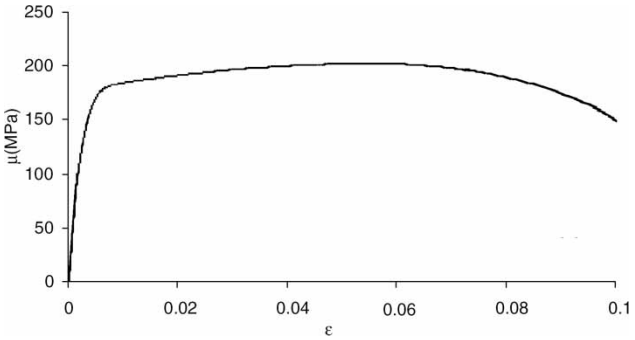

Fig. 1 True stress–true strain characteristic of the aluminium alloy (experimental)

Table 1 True stress–plastic strain data points used for aluminium in numerical simulations

σ (N/mm^2)	175	185	192	200	205	210
ε_p	0	0.01	0.02	0.03	0.04	0.05

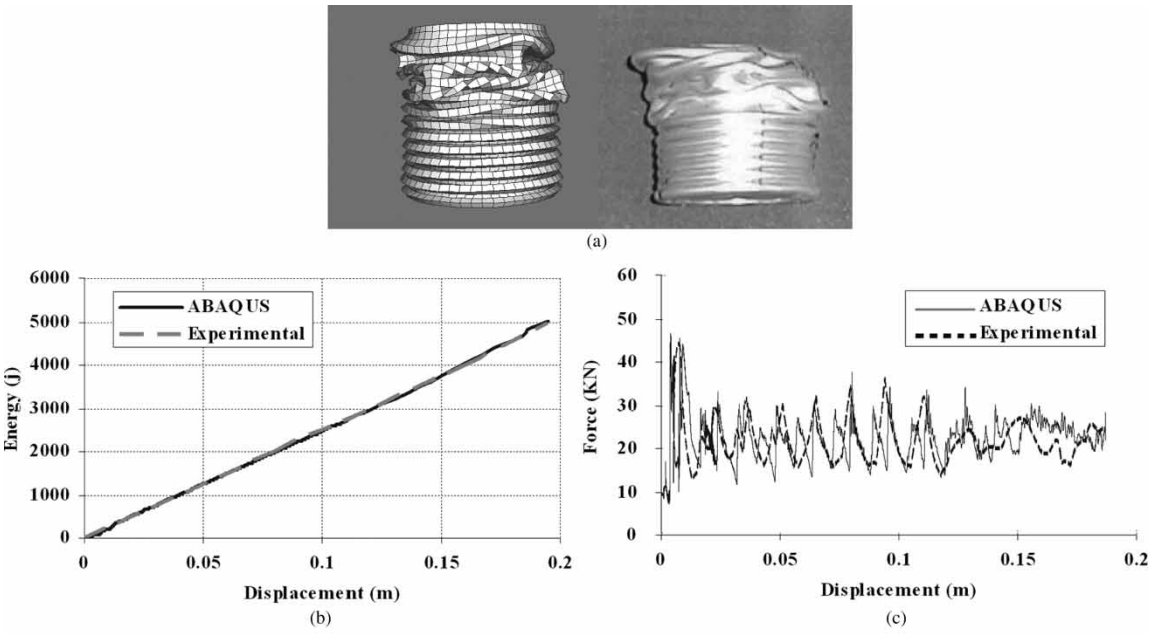

Fig. 2 Collapsing of a tube under axial quasi-static load obtained from the experimental [**5**] and numerical results. (a) The deformed shape, (b) the absorbed energy, and (c) reaction force against the axial deformation

2.2 Verification of the FE simulation using the previously reported experimental results

Crushing simulation of a tube under quasi-static axial loading is carried out and the results are compared with the experimental results of Hsu and Jones [**5**] in order to evaluate the accuracy of the FE simulation in predicting the absorbed energy and the crush force as well as the deformation mode of the tube. The tube has a nominal outer diameter of 50.8 mm (2 in), length of 250 mm, and a wall thickness of 1.53 mm. The tube is made of 6063-T6 aluminium alloy. The material properties of this alloy are described in reference [**5**]. The specimen is sandwiched between two parallel high-strength steel plates and the upper plate moves downward with a constant speed of 2 mm/min. The maximum axial deflection is set to 150 mm. Figure 2(a) shows the deformed shape obtained from the experimental and numerical results. The absorbed energy and crush force against the axial deformation of the tube obtained by the numerical simulation and experimental test are compared in Figs 2(b) and (c), respectively. As it is shown, the numerical simulation predicts closely the deformed shape as well as the absorbed energy and crush force.

2.3 Quasi-static crush test to verify the FE simulation

A quasi-static crush test is carried out to verify the accuracy of the numerical simulation results. In this test, an aluminium alloy tube of external diameter 75.6 mm, length of 151.2 mm, and a wall thickness of 1.4 mm is loaded quasi-statically in axial direction by using a compression testing machine at a nominal cross head-speed of 5 mm/min. In order to obtain the material data, a quasi-static material test is performed on a strip cut from a shell using a standard tensile test machine and the resulting stress–strain curve is used to introduce the approximated true stress-plastic strain data points in the numerical simulation. The specimen is placed between parallel steel plates of the test machine without any additional fixing. The maximum axial deflection is set to 105 mm. Figure 3 compares the experimental and numerical results of the deformed shape for the tube. Figure 4 shows the axial load against the axial deformation obtained from the experimental and numerical results. It is obvious that the numerical method simulates the crushing behaviour of the tube with sufficient accuracy.

3 THE INFLUENCE OF THE PLASTIC BUCKLING MODES ON THE COLLAPSING SHAPE OF THE TUBE

3.1 The influence of initial imperfection on the collapsing modes classification chart

Inasmuch as the tubes deformation under axial load will involve buckling, it is necessary to perturb the initial geometry of the tube in the crushing analysis proportional to the buckling modes. By ignoring the

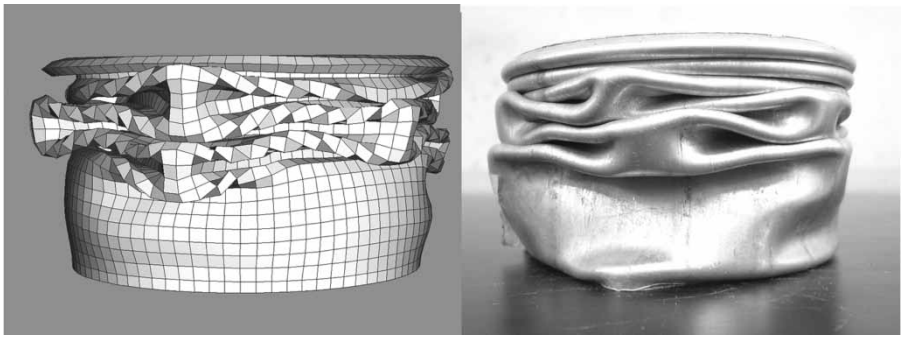

Fig. 3 The deformed shape of the tube under axial quasi-static load obtained from the experimental and numerical results

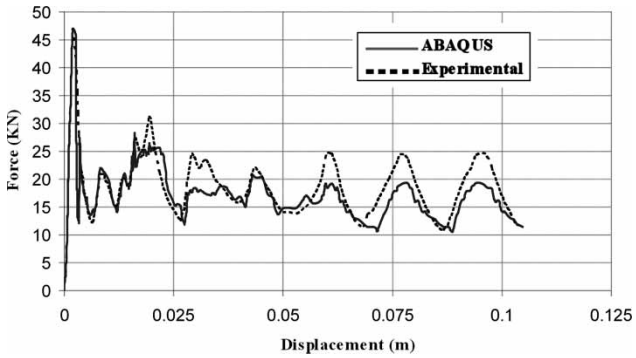

Fig. 4 The reaction force against the axial deformation of the tube under quasi-static load obtained from the experimental and numerical results

geometrical perturbation, numerical methods only predict the axisymmetric collapsing mode for all case studies because the geometrical model and load condition are both axisymmetric in collapsing of tubes under axial load. However, the experimental tests show that concertina collapsing happens only for a narrow range of tube dimensions. This phenomenon can be explained by considering an instantaneous buckling just before the crushing of tube. The effect of this initial buckling can be introduced in numerical simulation by applying an initial imperfection proportional to the buckling modes on the tube in crushing analysis. Experimental results show that the best geometrical imperfection for applying on the tube model in numerical simulation is a linear combination of some of the first buckling modes, for example the first ten plastic buckling modes [**13**]. Typically, the magnitude of the perturbation used for each eigenmode is a function of the relevant structural dimension, such as shell thickness and the magnitude of the corresponding eigenvalue. Since the lowest eigenmodes are most pertinent to the crushing behaviour of the structure, appropriate magnitudes may be found by obtaining a mesh imperfection of a few percent of the shell thickness for the first eigenmode and a decreasing percentage as the corresponding eigenvalue of modes increases. The magnitude of these imperfections are found by a trial and error procedure and comparing the results of numerical simulation with the experimental results. Note that the magnitudes related to the modes change proportional to the change of each eigenvalue related to the first eigenvalue, so the only unknown in each attempt of trial and error procedure is the imperfection proportional to the first mode. In this study, the magnitude for the first mode is set to 2 per cent of shell thickness that was previously reported in the literature too [**13**].

In order to perform the procedure of applying these imperfections on the structure, in each numerical simulation, the first ten buckling modes and their corresponding eigenvalues of the tube are obtained by running an eigenvalue buckling analysis using ABAQUS/Standard. As a sample, the first four buckling mode shapes of a tube of $D = 120\,\text{mm}$, $L = 216\,\text{mm}$, and $t = 2\,\text{mm}$ are shown in Fig. 5. These modes are related to buckling of the tube placed between two

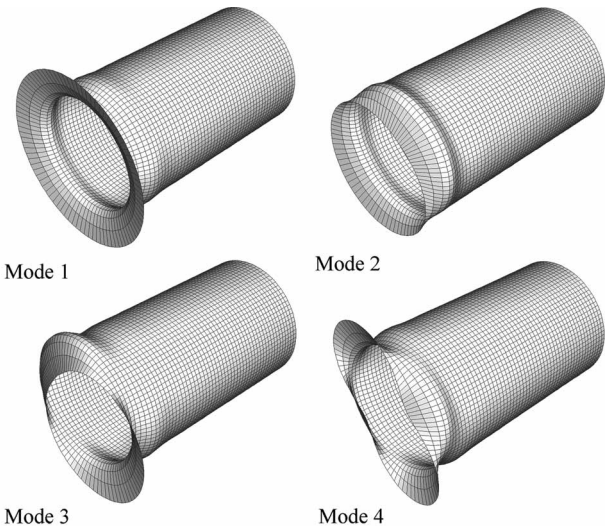

Fig. 5 The first four mode shapes of a tube subjected to axial compression

rigid walls (the rigid walls are eliminated in Fig. 5 in order to improve the clarity of picture), the back wall is constrained and an axial force is applied to the front tube. The results of buckling analysis are stored, and in the next step, the IMPERFECTION keyword is used in ABAQUS/Explicit to read the buckling modes from the stored data, scale them by the defined magnitudes, and perturb the nodal coordinates of the FE model before the crushing analysis.

All the previous studies in the literature concentrate on finding an initial geometric imperfection in numerical simulations in order to simulate the experimental collapsing shape of tube with a good accuracy. The contribution of this initial imperfection on the collapsing mode of tube and finding applied methods based on this imperfection to control the collapsing mode is not studied yet. In this paper, initial imperfection proportional to the plastic buckling modes is introduced as a new parameter that controls the collapsing shape of tube under axial impact load. By performing numerical simulations for tubes of various L/D and D/t ratios for the impact velocity $V_0 = 7$ m/s, the limits of the region in which the concertina crushing mode is guaranteed in the L/D–D/t diagram is obtained and shown in Fig. 6. The results of an experimental test in the case of quasi-static loading [**1**] are shown in this figure too. As it is shown, the limits of the concertina collapsing region for the crush simulations are similar to the results of quasi-static test. It is evident that, in both conditions of loading, only the tubes with relatively small L/D and D/t ratios that have a lower ability in dissipating the energy, compare to larger tubes, collapse in concertina mode.

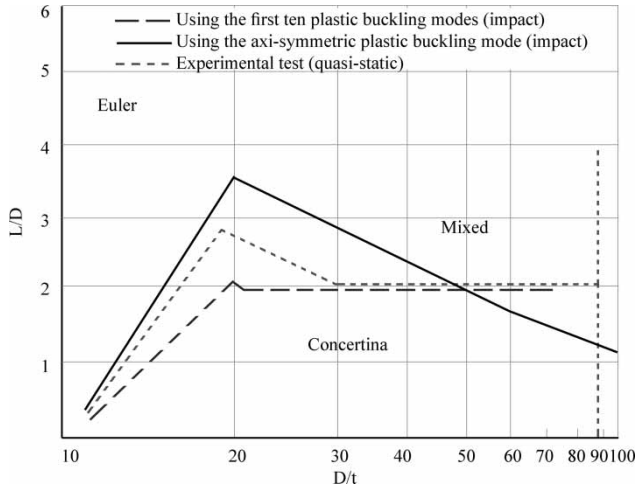

Fig. 6 The limits of the concertina collapsing region

In the next step, the same numerical simulations of tube crushing under axial impact load are performed, but solely the initial geometric imperfection of the axisymmetric buckling mode (like mode 1 in Fig. 5) is applied on the structure at the beginning of the crushing analysis. As it is shown in Fig. 6 the limits of the concertina collapsing mode region extend remarkably in the L/D–D/t diagram using this method, except for the tubes of relatively great diameters. This phenomenon reveals that by activating the axisymmetric buckling mode of the tube under axial compression, the concertina collapsing mode takes place for a wider range of dimensions. The following sections, describe applied design methods in order to activate the axisymmetric buckling mode.

3.2 Quasi-static crush tests to verify the collapsing modes classification chart

Six quasi-static crushing tests are performed in order to verify the classification chart presented in Fig. 6. According to this chart, numerical simulations predict concertina collapsing mode for tubes of any $20 < D/t < 75$ and L/D of two or less and predict mixed mode for L/D of two or greater in this range of D/t. The main purpose of this section is evaluating the numerical results for the classification chart in the range of $20 < D/t < 75$, so the tests are carried out for two different D/t ratios ($D/t = 54$ and 72) and three L/D ratios for each D/t value. The test conditions and material properties are the same as the test in section 2.3. The dimensions of tubes and the axial deflection for each test are shown in Table 2, note that the thickness of tube is set to 1.4 mm for all specimens.

Table 2 Results from the quasi-static experimental tests and numerical simulations

Test #	D/t	L/D	Deflection (mm)	F_{max} (kN)		F_{mean} (kN)		Mode[a]	
				Exp[b]	Num[b]	Exp	Num	Exp	Num
1	54	1	50	47.2	48.1	19.9	18.1	C	C
2	54	2	105	47.4	47.2	18.3	17.6	M3	M3
3	54	3	190	48.4	49.3	18.0	17.4	M3	M3
4	72	1.1	85	59.9	57.6	23.0	19.8	C	C
5	72	2	140	66.0	63.2	22.1	20.1	M4	M4
6	72	3	200	62.7	64.1	21.2	20/3	M4	M4

[a] C, concertina; M3, mixed mode with three circumferential lobes; M4, mixed mode with four circumferential lobes.
[b] Exp, experimental; Num, numerical.

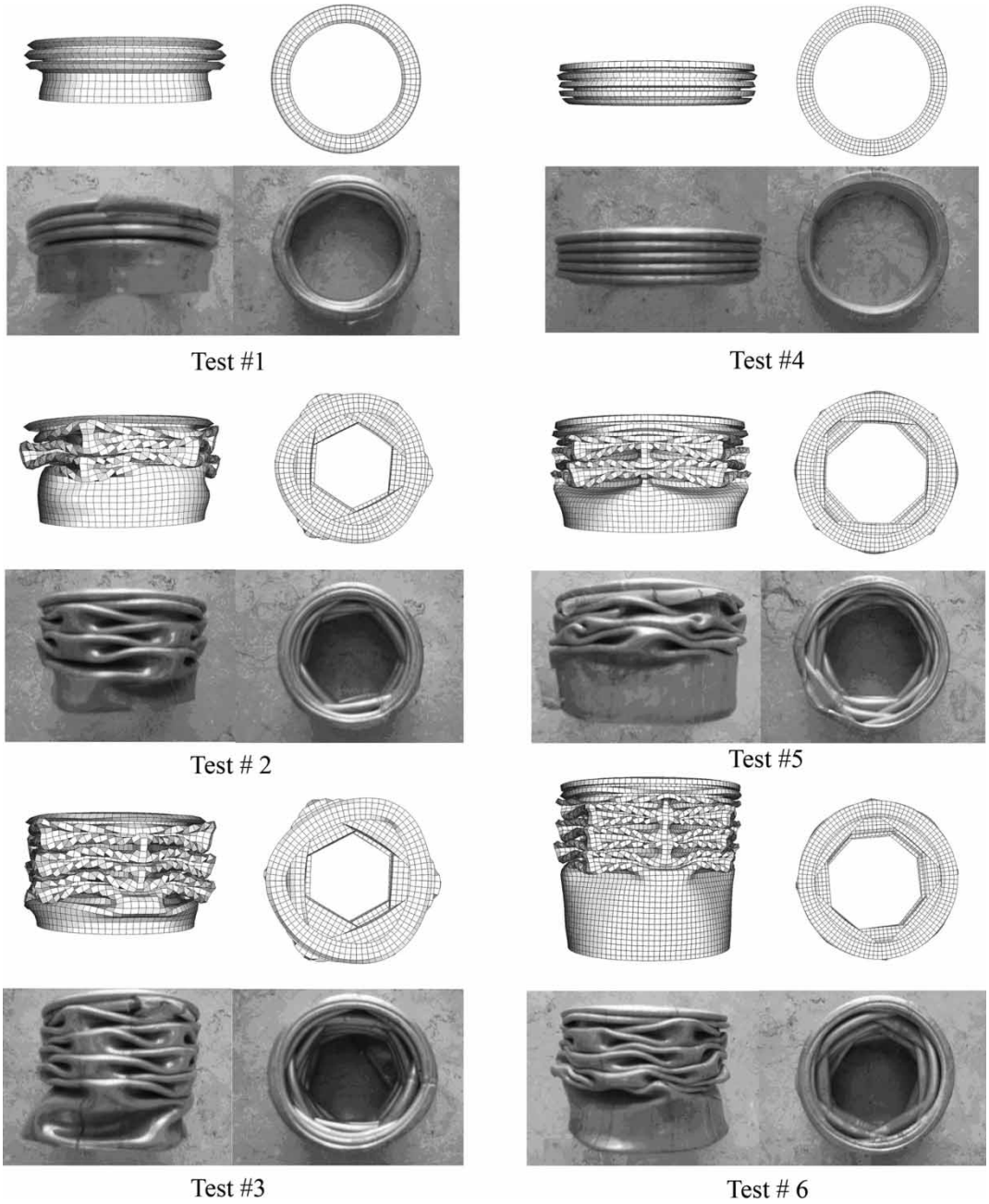

Fig. 7 Comparison of the results for tubes collapsing mode under axial quasi-static load obtained from experimental tests and numerical simulations

The collapsed shape of tube obtained by FE simulation and experimental tests are compared in Fig. 7 for these tests. It is obvious from the presented results that numerical method can simulate the collapsing shape of tube with sufficient accuracy. Table 2 shows the values of the maximum and mean collapsing force obtained from FE simulation and experimental tests. It is obvious from Fig. 7 and Table 2 that the numerical simulation can predict the collapsing shape and the crashworthiness parameters with a great accuracy.

4 TUBES WITH A CIRCUMFERENTIAL EDGE GROOVE

As it is shown in Fig. 5, in the axisymmetric buckling mode the edge ring of the tube deforms outwards. An applied design to activate this mode is weakening the edge ring of the tube by cutting a circumferential edge groove outside the tubes to force this ring to deform outwards at the beginning of the crushing.

Most of the previous reported works on designing the grooved tubes in order to control the collapsed shape under axial loading are restricted to the tubes with grooves alternately cut outside [**14**] or inside and outside [**15**] the tube or the spirally slotted tubes [**16**]. The common weakness of all these designs is in the reduction of the amount of material participating in the plastic deformation and energy absorption. However, in the presented design, as it will be shown in the following sections, the amount of material that does not contribute in energy absorption is so low that the groove have a negligible influence on the energy absorption capacity of the structure, on the other hand the presented design have a remarkable influence on the collapsed shape of the tube.

The edge grooves are of $W = 3$ mm wide and $d = 1$ mm depth. The details of the specimen design are given in Fig. 8. In order to model the specimen, the shell thickness of the first row of elements in the FE model is changed to $t = 1$ mm and the OFFSET parameter is used in the SHELL SECTION keyword, to adjust the position of this row of elements like Fig. 8. The procedure of extracting the buckling mode shapes and their corresponding eigenvalues, and the crush analysis is like before. Numerical simulations for tubes in the range of $20 < D/t < 100$ and $1 < L/D < 6$, before and after cutting the circumferential groove are performed and the limits of the concertina collapsing region are obtained. Figure 9 shows the remarkable extension of the axisymmetric collapsing region after cutting a circumferential edge groove on the tubes.

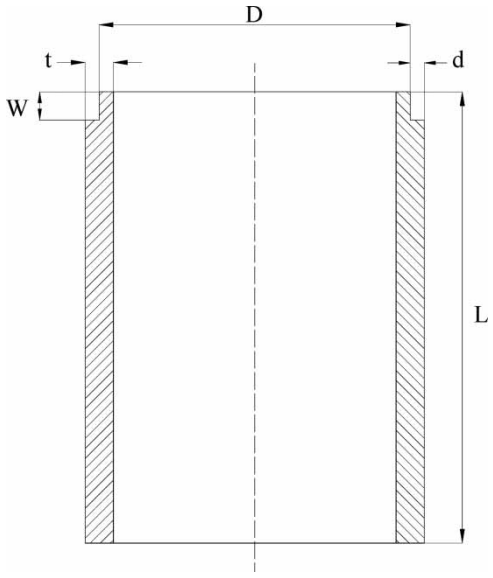

Fig. 8 Details of the circumferential groove design

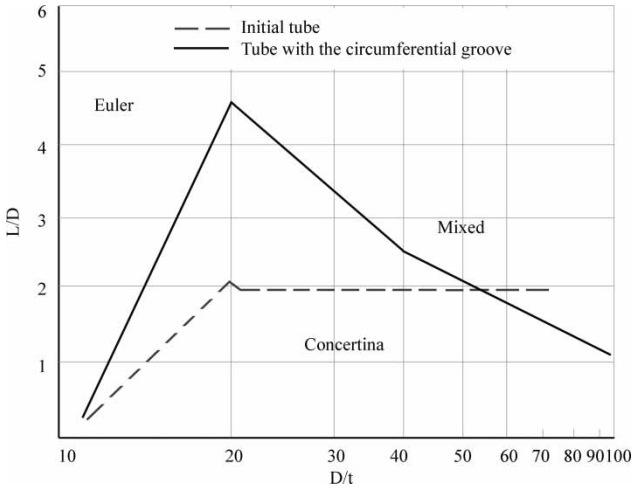

Fig. 9 The limits of the concertina collapsing region before and after cutting the circumferential groove

5 QUASI-STATIC EXPERIMENTAL TESTS ON TUBES WITH A CIRCUMFERENTIAL EDGE GROOVE

As explained in the previous section, cutting a circumferential edge groove on the tube activates the axisymmetric buckling mode and increases the probability of forming axisymmetric folds in contrast with diamond folds. In order to verify the numerical results, 16 experimental tests are carried out. These tests are performed on tubes with $D/t = 49$, $t = 2$ mm and four different L/D ratios. The material properties and test conditions are similar to those given in section 3.2. For each L/D and D/t ratio, two specimens with and without grooves are prepared. Figure 10 shows a specimen with the edge groove. The dimensions of groove are similar to that given

Fig. 10 A specimen with circumferential edge groove

in Fig. 8. Table 3 contains the properties of these eight specimens. In order to guaranty the accuracy of the experimental tests, each test was carried out two times. Figure 11 compares the collapsing mode of tubes with edge groove and the initial tubes. It is obvious that cutting the edge groove increases the number of axisymmetric folds. In all the tests for tubes with circumferential edge groove, after forming two or three axisymmetric folds the collapsing mode changes to diamond. This phenomenon may be because of non-symmetric deflections that are generated on the tube during cutting the edge groove. As shown in Table 3, cutting the edge groove decreases the value of maximum reaction force that is a great advantage in designing tubes as mechanical shock absorbers.

Table 3 Details of specimens used for studying the influence of cutting a circumferential edge groove on the collapsing mode (as shown in Fig. 11)

Test #	L/D	F_{max} (kN)	Number of axisymmetric folds
A	1.75	64.1	1
A-Groove	1.75	50.6	3
B	1.85	64.5	1
B-Groove	1.85	51.8	2
C	1.80	64.3	1
C-Groove	1.80	52.4	2
D	1.70	64.1	1
D-Groove	1.70	52.7	3

6 TUBES WITH ONE- AND TWO-CIRCUMFERENTIAL STIFFENERS

As another design for broadening the concertina collapsing region, the circumferential stiffeners may be added to the tube. In the first step, it is assumed that a stiffener ring is attached to the top ring of the tube as shown in Fig. 12. In order to model the specimen with the stiffener ring, a boundary condition that constrains the radial displacement of nodes on the edge of the tube is used. In the range of $20 < D/t < 100$ and $1 < L/D < 6$, the collapsing mode classification chart for the tubes before and after using the stiffener ring is depicted in Fig. 13. It is evident that the stiffener ring extends the concertina mode remarkably without influencing the energy absorption of the structure as it will be shown in the next section.

Another design to extend the concertina collapsing region is attaching two stiffener rings to the tube. The second stiffener is attached to the middle of the tube. The broadened limits of the concertina collapsing region for tubes with two stiffener rings are also shown in Fig. 13.

7 COMPARING THE CRASHWORTHINESS PARAMETERS OF THE PRESENTED DESIGNS

The absorbed energy, maximum and mean reaction forces, and maximum deflection in axial direction are the most important crashworthiness parameters in

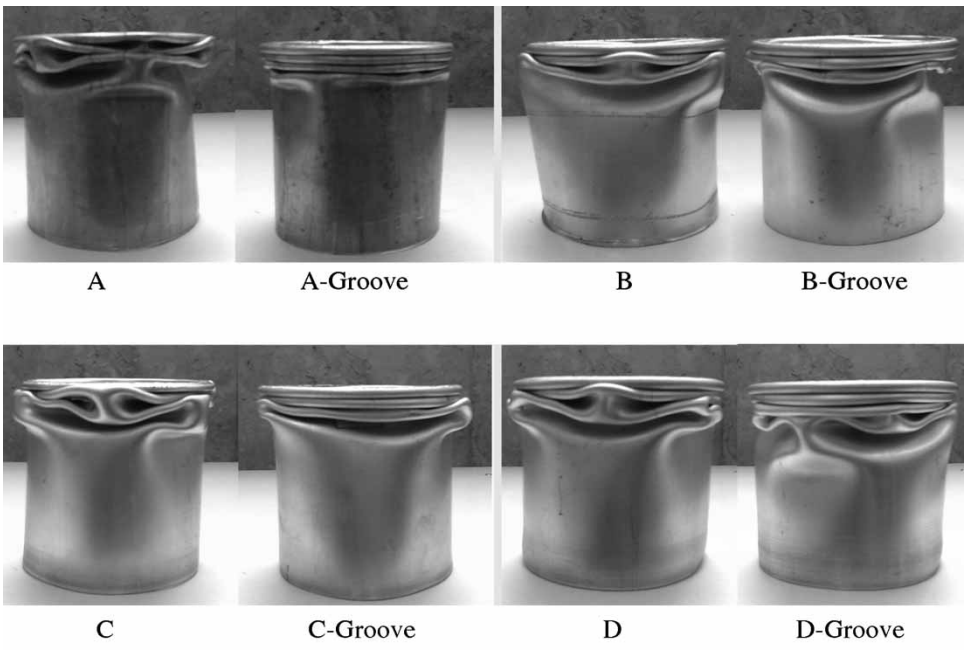

Fig. 11 The influence of cutting a circumferential edge groove on the collapsing mode of tubes under quasi-static axial load

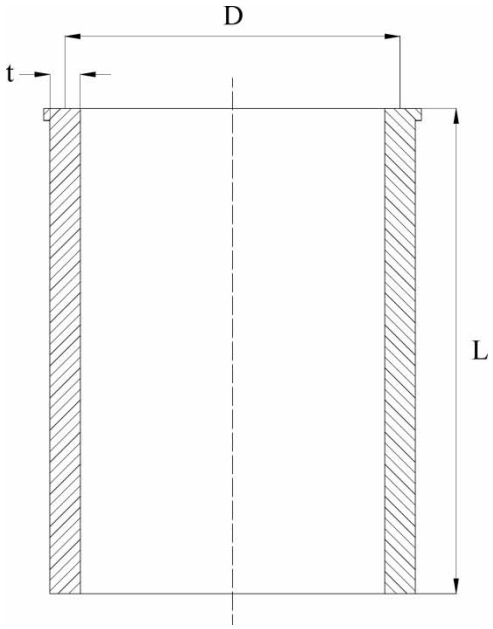

Fig. 12 Tube with the stiffener ring

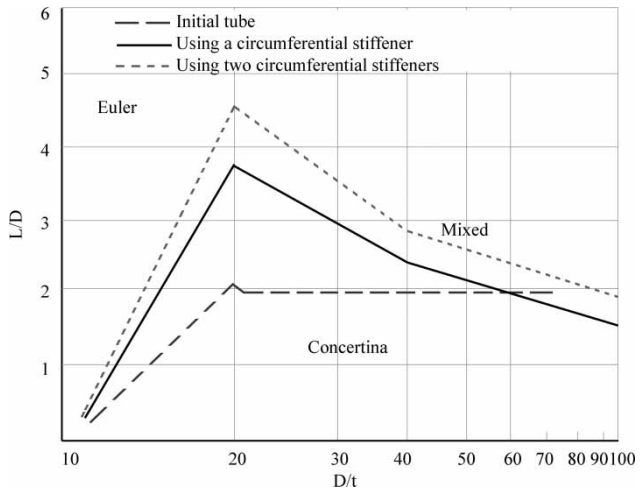

Fig. 13 Broadening of the concertina collapsing region using one- and two-stiffener rings

designing collapsible shock absorbers. These parameters are calculated in all the performed numerical simulations, as a sample these parameters are shown in Table 4 for tubes with $D/t = 20$ and three different L/D ratios. Table 5 contains the same results for tubes of $D/t = 40$. As expected, the absorbed energy for grooved tubes is less than the energy absorbed by a tube of the same dimensions with the stiffener ring. This phenomenon can be explained due to the amount of material that participates in dissipating the impact energy for these tubes. The amount of the absorbed energy against the axial deflection is shown in Fig. 14 for a tube of $D/t = 40$ and $L/D = 2.3$ with one stiffener ring and with the circumferential edge groove, as it is shown, the absorbed energy of the grooved tube falls down during the formation of the first fold. It is evident that the difference between the absorbed energy for these tubes is almost negligible and the designer may chose any of these suggestions depending on the ease of manufacture. Comparison of the maximum and mean reaction forces for tubes of relatively great D/t ratios ($D/t \geqslant 40$) shows that using the circumferential groove can reduce the peak reaction force that happens at the beginning of the crushing. The reduction of the reaction force can be considered as a remarkable advantage for the grooved tubes design.

8 NEURAL NETWORK SYSTEMS TO REPRODUCE THE CRUSH BEHAVIOUR OF THE TUBE

The idea of using the artificial neural networks originates from the fact that all the biological neural functions, including memory, are stored in the neurons and in the connections between them. In other words, learning may be defined as the establishment of new connections between neurons or the modification of existing connections [**17**]. The artificial neural networks are a simple set of computing units or neurons that can be trained to reproduce the behaviour of a complex function.

The background work in the field of neural networks occurred in the late 19th and early 20th centuries. Among different kind of problems, the idea of using neural networks in engineering problems was first developed in 1940s by Warren McCulloch and Pitts [**18**] who showed that the neural network systems can compute any arithmetic or logical function. During the recent years, the application of neural network systems is expanded to a vast range of problems in addition to the engineering or mathematic fields, like business, medicine, finance, and literature, inasmuch as the neural networks are not programmed to solve a specific kind of problems. Indeed, the neural network systems are not influenced by the physic equations of a problem, they only work by training themselves using the past results of a problem and adapting their computing units to solve the new problems of the same kind.

In the present study neural network systems are used to reproduce the crush behaviour of thin-walled tubes. In the previous sections, all the results were obtained from the FE simulations, but the final goal of the following sections is optimization of the tube dimensions under crashworthiness requirements. In order to achieve this, the optimization procedure, that uses an iterative algorithm, needs the results of several simulations. Performing all these simulations by the FE method is very expensive and time consuming from the computational point of view. To challenge this

Table 4 Comparison of the crashworthiness parameters for tubes with one stiffener ring and grooved tubes of $D/t = 20$

	20-3		20-3.5		20.4	
D/t–L/D	Edge groove	One stiffener ring	Edge groove	One stiffener ring	Edge groove	One stiffener ring
Absorbed energy (J)	2270	2364	2991	3141	3435	3448
δ_{max} (cm)	8.39	8.3	11.03	10.9	12.24	12.21
F_{max} (KN)	54.31	46.15	59.86	46.24	46.07	46.06
F_{mean} (KN)	27.06	28.21	27.11	28.8	28.12	28.21

Table 5 Comparison of the crashworthiness parameters for tubes with one stiffener ring and grooved tubes of $D/t = 40$

	40-2		40-2.3		40-2.5	
D/t–L/D	Edge groove	One stiffener ring	Edge groove	One stiffener ring	Edge groove	One stiffener ring
Absorbed energy (J)	4501	4704	5674	5914	6125	6125
δ_{max} (cm)	12.85	11.87	14.18	14.38	15.80	15.84
F_{max} (KN)	83.28	85.38	77.60	87.53	81.11	93.54
F_{mean} (KN)	35.02	39.65	40.01	41.12	38.76	38.66

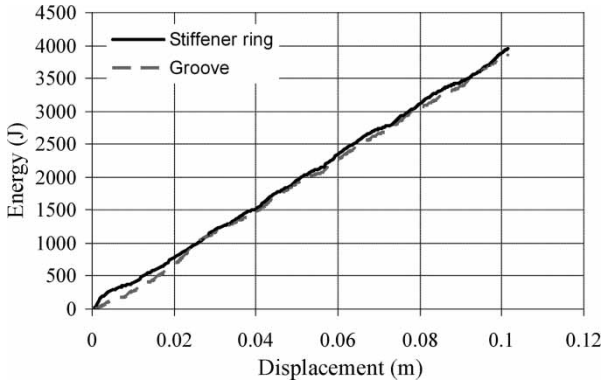

Fig. 14 Comparison of the absorbed energy for a tube with one stiffener ring and a grooved tube

problem, a set of neural network systems is developed and trained by a limited number of FE simulations.

The response of the structure to impact load is often non-smooth and highly non-linear with respect to the variables of the problem like the dimensions, boundary conditions, and impact velocity. Indeed, developing a single artificial neural network to reproduce all the crashworthiness parameters of the structure simultaneously with sufficient accuracy is impossible, so in the present study different systems of neural networks are developed in order to reproduce the crashworthiness parameters of the tube, separately. Furthermore, because the high non-linearity of the problem, the optimization algorithm is highly sensitive to the accuracy of the approximated results obtained by the developed neural networks, so, in order to achieve the desired accuracy, for some of the crashworthiness parameters two parallel networks are developed and the final value of the parameter is obtained by averaging the output values of each combination of networks.

In this work, only multi-layer perceptron (MLP) neural networks are used [**17**]. The MLPs are currently the most widely used neural networks in engineering problems. A schematic of a two-layer perceptron network with one neuron in each layer is shown in Fig. 15. An MLP network can have an arbitrary number of layers with different transfer functions in each layer, the output of each layer is the input of the next layer, and each layer may have a different number of neurons. For each neuron, the input is weighted with an appropriate value that is shown in the figure by W. The sum of the weighted input and the bias (b) forms the input to the transfer function f. Neurons may use any differentiable transfer function f to generate their output [**19**]. The output layer has a number of neurons equal to

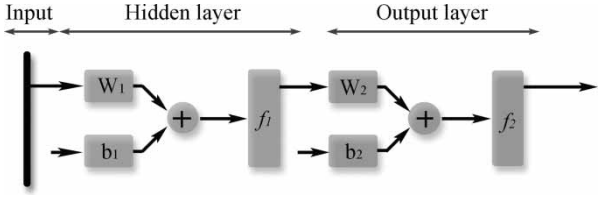

Fig. 15 Schematic of a two-layer perceptron network

the number of output variables. The MLP neural networks are called the feed forward networks because as it is shown in Fig. 15 the signals always propagate from the first to the last line of neurons. Indeed, for an MLP network, the learning is performed by adjusting the weights of the neurons such that the RMS error between the known outputs of the training set and the network returned outputs are minimized.

9 NEURAL NETWORKS DEFINITION

In the present study, the design variables are set to the L/D and D/t ratios, the aim of designing the network systems is reproducing the most important crashworthiness parameters of the tube as a shock absorber that are, the specific absorbed energy (the absorbed energy per unit volume), the maximum axial displacement of the tube, the maximum reaction force and the mean reaction force. Four different neural network systems are developed in order to be used for these parameters, furthermore some of these four systems contain two parallel neural networks and the final output for each parameter is calculated by averaging the output of the parallel networks. The schematic of developed neural network system is shown in Fig. 16.

The details of the neural network design, containing the number of neurons and the transfer function in each layer are explained in Table 6. The Levenberg–Marquardt algorithm is used for training all the neural networks [**17**].

10 TRAINING AND TEST SETS

The final performance of the neural networks is highly sensitive to the settlement of the training sets in the design variables domain. A general rule for choosing the location of the training sets in the design variables domain is not still achieved and there are several methods like random allocation of sets [**12**, **20**] or regular arrangement of sets.

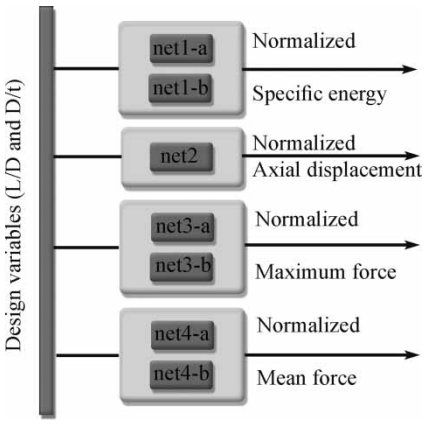

Fig. 16 The designed neural network system for reproducing the crashworthiness parameters of the tube

In the present study, the training and test sets are defined regularly in the range of $20 < D/t < 60$ and $1 < L/D < 4$, that will be the optimization domain too. Neural networks are developed to reproduce the crush behaviour of the initial tube and the tube with one stiffener ring. Total of 48 FE simulations are performed (24 for the initial tube and 24 for the stiffened tube with one ring), among these, 40 runs are considered as the training set and the test set contains eight FE runs. The values of the most important crashworthiness parameters of the tube, containing the specific absorbed energy, the maximum axial displacement of the tube, the maximum reaction force and the mean reaction force are calculated by FE simulations. The normalized specific absorbed energy with respect to the maximum value of this parameter in the training set domain that is 77 748 KJ/m^3 is shown in Fig. 17(a) for a tube with the stiffener ring, and the normalized axial deflection of the stiffened tube with respect to the maximum deflection in training set (that is 16.59 cm) is shown in Fig. 17(b). The values of the maximum reaction force and the mean reaction forces for the training set of the stiffened tube are shown in Tables 7 and 8, respectively. The values of the crashworthiness parameters in the

Table 6 Details of the neural network system design

		First layer		Second layer		Third layer	
		Neurons	Transfer function	Neurons	Transfer function	Neurons	Transfer function
Specific energy (e)	Net1-a	4	tansig	4	tansig	1	purelin
	Net1-b	5	tansig	3	tansig	1	purelin
δ_{max}	Net2-a	6	tansig	4	tansig	1	purelin
F_{max}	Net3-a	6	tansig	3	logsig	1	purelin
	Net3-b	6	tansig	4	tansig	1	purelin
F_{mean}	Net4-a	8	tansig	7	logsig	1	purelin
	Net4-b	4	tansig	4	logsig	1	purelin

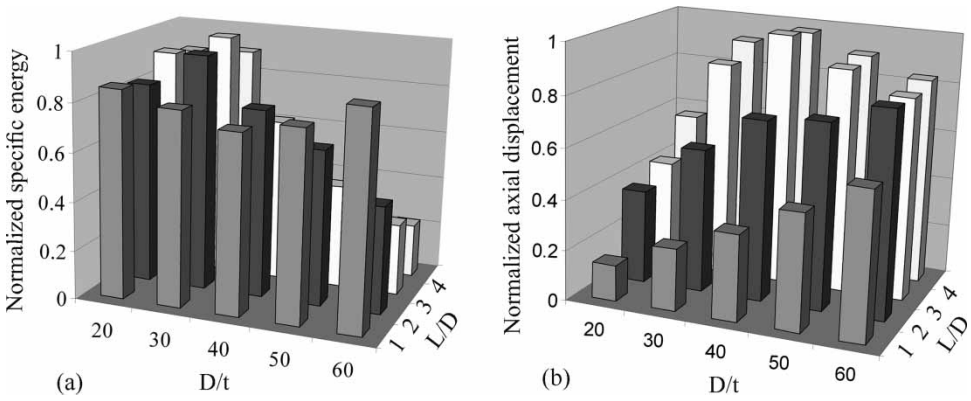

Fig. 17 The normalized values of (a) the specific energy and (b) the maximum axial deflection for the training set, the stiffened tube

Table 7 The training set for f_{max}, tube with the stiffener ring (KN)

L/D	$D/t = 20$	$D/t = 30$	$D/t = 40$	$D/t = 50$	$D/t = 60$
1	46.74	69.27	85.59	110.24	129.16
2	46.26	68.58	85.38	122.65	135.38
3	46.15	68.03	88.67	111.45	127.56
4	46.06	68.09	91.20	112.66	133.82

Table 8 The training set for f_{mean}, tube with the stiffener ring (KN)

L/D	$D/t = 20$	$D/t = 30$	$D/t = 40$	$D/t = 50$	$D/t = 60$
1	29.99	33.56	39.56	42.31	48.09
2	28.88	35.68	38.24	42.72	45.29
3	28.82	36.00	36.90	42.58	46.20
4	27.28	34.79	38.28	40.63	43.55

training set of the initial tube are shown in Tables 9 to 12.

After training all the networks, the test sets are used to find the error of each network. As a sample, Fig. 18 shows the error between the maximum and mean reaction force obtained by the FE method and the trained neural network system. As it is shown the maximum error for the reaction forces is about 5.5 per cent.

Table 9 The training set for e, the initial tube (KJ/m^3)

L/D	$D/t = 20$	$D/t = 30$	$D/t = 40$	$D/t = 50$	$D/t = 60$
1	65 861	56 939	55 679	57 604	68 844
2	66 856	72 580	55 832	49 736	34 422
3	66 594	77 215	52 074	33 157	22 948
4	66 777	70 030	39 055	24 868	17 211

Table 10 The training set for δ_{max}, the initial tube (cm)

L/D	$D/t = 20$	$D/t = 30$	$D/t = 40$	$D/t = 50$	$D/t = 60$
1	2.87	3.98	5.69	7.61	9.98
2	5.08	8.74	13.09	13.43	12.88
3	8.31	13.83	15.4	14.64	13.14
4	8.97	14.94	15.12	14.67	12.95

Table 11 The training set for f_{max}, the initial tube (KN)

L/D	$D/t = 20$	$D/t = 30$	$D/t = 40$	$D/t = 50$	$D/t = 60$
1	48.64	69.93	92.65	110.68	137.18
2	50.05	67.84	90.14	122.54	139.22
3	48.49	67.44	88.16	112.68	131.40
4	45.08	68.73	61.86	111.29	135.52

Table 12 The training set for f_{mean}, the initial tube (KN)

L/D	$D/t = 20$	$D/t = 30$	$D/t = 40$	$D/t = 50$	$D/t = 60$
1	25.65	33.16	40.23	46.26	49.32
2	30.04	36.13	39.94	46.54	48.33
3	30.42	36.43	39.01	42.42	47.74
4	27.97	36.66	40.84	44.57	47.35

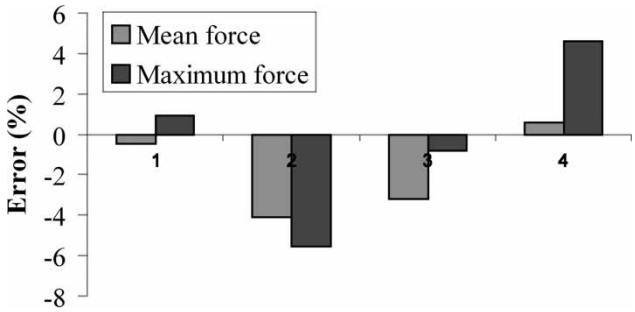

Fig. 18 Errors of the neural network for the reaction forces in test set, tube with the stiffener ring

11 THE RESPONSE SURFACES

Using the trained neural networks, the values of the crashworthiness parameters as a function of the design variables (L/D and D/t ratios) are calculated for the initial tube and the tube with the stiffener ring. Figure 19 shows the normalized values of these parameters with respect to the maximum value of each parameter in the training set for the stiffened tube with one ring. The highly non-linear behaviour of the specific absorbed energy is demonstrated in Fig. 19(a), but the behaviour of the maximum axial deflection, the maximum reaction force and the mean reaction force appears more regular and smooth. Figure 19(b) shows that the maximum axial deflection of the tube under impact load increases for the greater values of L/D and D/t ratios and then remains almost constant for the L/D and D/t ratios greater than 2 and 30, respectively.

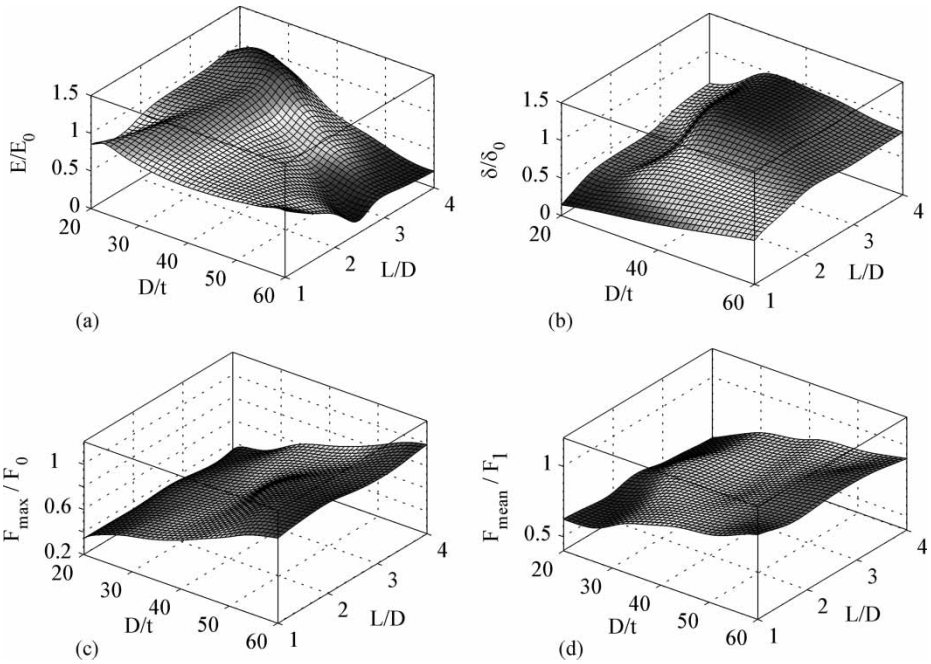

Fig. 19 The response surfaces for the crashworthiness parameters of the tube with the stiffener ring

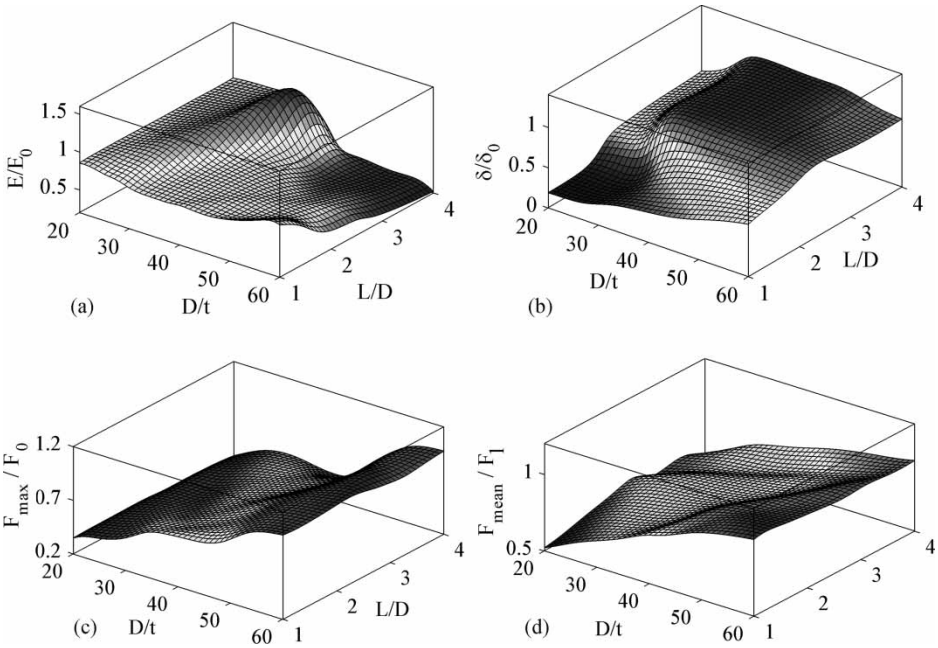

Fig. 20 The response surfaces for the crashworthiness parameters of the initial tube

It is evident from Figs 19(c) and (d) that the reaction forces are almost independent from the L/D ratio and increase monotonically by increase of the D/t ratio. The same response surfaces for the crashworthiness parameters of the initial tube are shown in Fig. 20.

12 CRASHWORTHINESS OPTIMIZATION

12.1 Problem formulation

Several problems of crashworthiness optimization may be considered even for a simple structure under impact load. Due to the variety of the parameters that influence the response of the structure subjected to dynamic loading, different classes of the optimization problems may be introduced. However, generally the problem can be formulated as

$$\text{optimize:} \quad \{F(x)\} \tag{1}$$

$$\text{subjected to:} \quad g_i(x) \leqslant 0 \quad i = 1, \ldots, N_c \tag{2}$$

$$\text{within the design space:} \quad x_{il} \leqslant x_i \leqslant x_{iu} \quad i = 1, \ldots, N_d \tag{3}$$

where $F(x)$ is the objective or fitness function, $g_i(x)$ are the constraint functions, and x_i are the design variables. The parameters x_{il} and x_{iu} are the lower and upper bounds of the design variable domain. In the present study the design variables are set to the dimensions of the tube or L/D and D/t ratios, the design variable domain is $20 < D/t < 100$ and $1 < L/D < 4$. Both the SO problem and the MO optimizations are performed by introducing different crashworthiness parameters as the objective function.

12.2 Genetic algorithm

The GA is an optimization method based on the process of evolution in biological population. In the GA, in the first step, a random population in the design variable domain is generated and in the next steps, successively new populations are produced using the previous individuals in such a manner that each new population is modified and evolves towards an optimal solution. For the crashworthiness problems that the objective function is highly non-linear with respect to the design variables, unlike the other standard optimization methods, the GA can be applied with sufficient accuracy.

In order to optimize the most important crashworthiness parameters of the structure that are the specific absorbed energy, the maximum axial deflection and the crush force efficiency, two different objective functions are generated by the weighted sum method as

$$f_1 = \left[K_1 \cdot \left(\frac{F_{mean}}{F_{max}} \right) + K_2 \cdot \left(\frac{E}{V} \right) \right] \tag{4}$$

$$f_2 = \left[n_1 \cdot \delta_{max} + n_2 \cdot \left(\frac{E}{V} \right) \right] \tag{5}$$

where k_1, k_2, n_1, and n_2 are the weighting parameters, E is the absorbed energy, V is the volume of the tube, δ_{max} is the maximum axial deflection, and f_{mean} and f_{max} are the mean and maximum reaction forces, respectively. The parameter f_{mean}/f_{max} is called the crush force efficiency. The high crush force efficiency allows the minimization of the difference between the mean force and maximum force and leads to limiting the peak of the acceleration. The final aim is maximization of the presented objective functions with different values of the weighting parameters. The appropriate values of the weighting parameters are very problem dependent and depend on the requirements of the design. In each of the presented objective functions, the SO problem can readily be obtained by setting one of the weighting parameters to zero and the other parameter to one. The optimization procedure for both of the objective functions for the initial tube and the stiffened tube are carried out with different values of the weighting parameters and the results are presented in Tables 13 and 14. It is evident that for the initial tube, in both of the objective functions the specific absorbed energy dominates the other crashworthiness parameters and the optimum point for different values of the weighting parameters is near the maximum point of the specific absorbed energy. For the tube with the stiffener ring, by increasing the weighting parameter of the specific absorbed energy and decreasing the weight of the crush force efficiency in the first objective function (f_1) the optimum point happens for the tubes of relatively greater D/t and L/D ratios. The optimization

Table 13 The optimization results for the objective function f_1, the initial tube and the tube with the stiffener ring

		Tube with the stiffener ring		Initial tube	
k_1	k_2	Optimum D/t	Optimum L/D	Optimum D/t	Optimum L/D
1	0	20.02	3.48	40.49	3.98
0.9	0.1	20.12	3.55	40.18	3.84
0.8	0.2	20.3	3.63	35.90	3.62
0.7	0.3	26.13	3.67	35.76	3.59
0.6	0.4	26.66	3.66	35.81	3.56
0.5	0.5	26.83	3.64	35.46	3.55
0.4	0.6	27.19	3.64	35.67	3.55
0.3	0.7	28.35	3.55	35.49	3.48
0.2	0.8	27.42	3.62	35.55	3.55
0.1	0.9	27.75	3.63	35.55	3.53
0	1	27.65	3.63	35.46	3.56

Table 14 The optimization results for the objective function f_2, the initial tube and the tube with the stiffener ring

		Tube with the stiffener ring		Initial tube	
n_1	n_2	Optimum D/t	Optimum L/D	Optimum D/t	Optimum L/D
1	0	37.29	3.31	39.93	3.29
0.9	0.1	35.43	3.46	35.80	3.56
0.8	0.2	34.19	3.49	35.69	3.54
0.7	0.3	33.40	3.51	35.68	3.55
0.6	0.4	32.24	3.54	35.67	3.55
0.5	0.5	31.52	3.55	35.62	3.54
0.4	0.6	30.53	3.54	35.67	3.54
0.3	0.7	29.32	3.59	35.46	3.58
0.2	0.8	28.69	3.61	35.53	3.53
0.1	0.9	27.89	3.63	35.47	3.54
0	1	27.80	3.63	35.46	3.56

results for the second objective function (f_2) show that by increasing the corresponding weighting parameter of the specific absorbed energy and decreasing the weight of the maximum axial deflection, the optimum D/t ratio decreases, whereas the L/D ratio increases. The presented results in Tables 13 and 14 can be used in designing the mechanical shock absorbers in the form of thin-walled tubes. The weighting parameters should be chosen proportional to the requirements of the design.

13 CONCLUSIONS

The current paper introduces the initial geometric imperfection proportional to the plastic buckling modes as a new parameter that can control the collapsing shape of the tube under impact loads. Numerical simulations are performed to find the influence of the presented parameter on the final collapsing shape of tubes with different dimensions. Two applied design methods use the presented parameter and numerical simulations are carried out to find the broadening of the region in the L/D–D/t diagram in which the concertina collapsing mode is guaranteed. Experimental tests are carried out to verify the accuracy of the numerical simulation.

Neural network systems are developed to reproduce the crashworthiness parameters of the structure and response surfaces of these parameters are portrayed using the trained neural networks. There are several parameters in designing neural network systems that can affect the accuracy of the results after training the network. Some of these parameters such as the exact number of layers and the number of neurons in each layer are obtained from an unavoidable error and trial procedure. In this study, appropriate designs of neural networks for reproducing the different crashworthiness parameters are presented in detail that can be used in a design office. In addition, the proposed response surfaces can be used in designing procedure directly.

In order to find the optimum L/D and D/t ratios, two different MO optimization problems are defined and designing tables are presented to find the optimum dimensions of the tube for different weighting parameters in the objective functions that can be chosen depends on the requirements of the design.

REFERENCES

1 **Guillow, S. R., Lu, G.,** and **Grzebieta, R. H.** Quasi-static axial compression of thin-walled circular aluminum tubes. *Int. J. Mech. Sci.*, 2001, **43**, 2103–2123.

2 **Karagiozova, D.** and **Alves, M.** Transition from progressive buckling to global bending of circular shells under axial impact – part I: experimental and numerical observations. *Int. J. Solids Struct.*, 2004, **41**, 1565–1580.

3 **Al Galib, D.** and **Limam, A.** Experimental and numerical investigation of static and dynamic axial crushing of circular tubes. *Thin-Walled Struct.*, 2004, **42**, 1103–1137.

4 **Karagiozova, D.** and **Jones, N.** Dynamic buckling of elastic–plastic square tubes under axial impact-2: structural response. *Int. J. Impact Eng.*, 2004, **30**, 167–192.

5 **Hsu, S. S.** and **Jones, N.** Quasi-static and dynamic axial crushing of thin-walled circular stainless steel, mild steel and aluminum alloy tubes. *Int. J. Crashworthiness*, 2004, **9**(2), 195–217.

6 **Vafa, J. P. M.** *Theoretical and experimental analysis of metal tubes under axial loading*. MSc Thesis, Amirkabir University of Technology (Tehran Polytechnic), 2006.

7 **Murase, K.** and **Wada, H.** Numerical study on the transition of plastic buckling modes for circular tubes subjected to an axial impact load. *Int. J. Impact Eng.*, 2004, **30**(8/9), 1131–1146.

8 **Karagiozova, D., Alves, M.,** and **Jones, N.** Inertia effects in axi-symmetrically deformed cylindrical shells under axial impact. *Int. J. Impact Eng.*, 2000, **24**, 1083–1115.

9 **Karagiozova, D.** and **Jones, N.** Influence of stress waves on the dynamic progressive and dynamic plastic buckling of cylindrical shells. *Int. J. Solids Struct.*, 2001, **38**, 6723–6749.

10 **Shakeri, M., Alibeigloo, A.,** and **Ghajari, M.** Numerical analysis of axi-symmetric collapse of cylindrical tubes under axial loading. In Proceedings of the Seventh International Conference of Computational Structures Technology (CST), (Ed. B. H. V. Topping) Civil-Comp Press, Lisbon, Portugal, 2004, paper 250.

11 **Kurtaran, H., Eskandarian, A., Marzoughi, D.,** and **Bedewi, N. E.** Crashworthiness design optimization using successive response surface approximations. *Comput. Mech.*, 2002, **29**, 409–421.

12 **Lanzi, L., Bisagni, C.,** and **Ricci, S.** Neural network systems to reproduce crush behavior of

structural components. *Comput. Struct.*, 2004, **82**, 93–108.
13 *Hibbit, Karlsson, Sorensen, Inc. Getting started with ABAQUS/Explicit version 6.3*, 2002 (HKS, USA).
14 **Mamalis, A. G., Manolakos, D. E., Ioannidis, M. B., Kostazos, P. K.,** and **Kastanias, S. N.** Numerical modeling of the axial plastic collapse of externally grooved steel thin walled tubes. *Int. J. Crashworthiness*, 2003, **8**(6), 583–590.
15 **Hosseinipour, S. J.** Mathematical model for thin-walled grooved tubes under axial compression. *Mater. Des.*, 2003, **24**, 463–469.
16 **Kormi, K., Wijayathunga, V. N., Webb, D. C.,** and **Al-Hassani, S. T. S.** FE investigation of a spirally slotted tube under axially compressive static and dynamic impact loading. *Int. J. Crashworthiness*, 2003, **8**(5), 421–431.
17 **Hagan, M. T., Demuth, H. B.,** and **Beale, M.** *Neural networks design*, 1996 (PWS Publishing Company, Boston, MA).
18 **McCulloch, W. S.** and **Pitts, W. H.** A logical calculus of ideas immanent in nervous activity. Bulletin of Mathematical Biophysics, selected papers on optical neural networks, 1943, vol. 96(5), pp. 115–133.
19 *Neural network toolbox, user's guide. MATLAB 7*, 2004 (Math Works, Inc.).
20 **Bisagni, C., Lanzi, L.,** and **Ricci, S.** Optimization of helicopter subfloor components under crashworthiness requirements using neural networks. *J. Aircr.*, 2002, **22**(2), 269–304.

APPENDIX

Notation

b_i	neuron's bias
D	tube diameter
E, e	absorbed energy and absorbed energy per unit volume
E_0	maximum value of the absorbed energy in the training set
f_i	transfer function of the ith layer
f_0	maximum value of $F_{\max}$ in the training set
f_1	maximum value of F_{mean} in the training set
$F_{\max}$, F_{mean}	maximum reaction force and mean reaction force
k_1, k_2, n_1, n_2	weighting parameters
L	tube length
t	wall thickness
W, d	circumferential groove's wide and depth
W_i	neuron's weight
x_i	design variables
$\delta_{\max}$	maximum axial deflection
δ_0	maximum value of the axial deflection in the training set

Copyright of Proceedings of the Institution of Mechanical Engineers -- Part C -- Journal of Mechanical Engineering Science is the property of Professional Engineering Publishing and its content may not be copied or emailed to multiple sites or posted to a listserv without the copyright holder's express written permission. However, users may print, download, or email articles for individual use.